Theoretical and experimental investigation of electron collisions with acetone

M. G. P. Homem,[1] I. Iga,[1] L. A. da Silva,[1] J. R. Ferraz,[2] L. E. Machado,[2] G. L. C. de Souza,[3] V. A. S. da Mata,[3] L. M. Brescansin,[4] R. R. Lucchese,[5] and M.-T. Lee[1]

[1]*Departamento de Química, UFSCar, 13565-905 São Carlos, São Paulo, Brazil*
[2]*Departamento de Física, UFSCar, 13565-905 São Carlos, São Paulo, Brazil*
[3]*Departamento de Química, UFMT, 78060-900 Cuiabá, Mato Grosso, Brazil*
[4]*Instituto de Física "Gleb Wataghin," UNICAMP, 13083-970 Campinas, São Paulo, Brazil*
[5]*Chemistry Department, Texas A&M University, College Station, Texas 77842-3012, USA*

(Received 2 August 2015; published 21 September 2015)

We report a joint theoretical-experimental investigation on elastic electron scattering by acetone in the low- and intermediate-energy regions. More specifically, experimental differential, integral, and momentum-transfer cross sections are given in the 30–800 eV and 10°–120° ranges. Theoretical cross sections are reported in the 1–500 eV interval. The experimental differential cross sections were determined using a crossed electron-beam–molecular-beam geometry, whereas the absolute values of the cross sections were obtained using the relative-flow technique. Theoretically, a complex optical potential derived from a Hartree-Fock molecular wave function was used to represent the collision dynamics, and a single-center expansion method combined with the Padé approximant technique was used to solve the scattering equations. Our experimental cross-section data are in generally good agreement with the present calculated data. Also, our calculated grand-total and total absorption cross sections are in good agreement with the experimental results reported in the literature. Nevertheless, our calculations have revealed a strong shape resonance in the $^2B_2$ scattering channel not clearly seen in the experimental results. Possible reasons for this fact are also discussed.

DOI: 10.1103/PhysRevA.92.032711 PACS number(s): 34.80.Bm

I. INTRODUCTION

From a theoretical point of view, electron-assisted processes involving the organic molecules with the carbonyl group in their structures may support a shape resonance due to the existence of an empty π^* orbital that may trap electrons to form metastable states. Such resonances were in fact identified in the theoretical studies of low-energy electron collisions with formaldehyde [1–3], formic acid [4,5], and, more recently, acetaldehyde [6] and formamide [7]. Experimentally, such resonances were seen in studies involving electron interaction with carbonyl-containing compounds. For instance, π^* shape resonances in the vibrational excitation cross sections (VECS) for electron scattering by formaldehyde were reported by Benoit and Abouaf [8]. For acetaldehyde, such resonances in VECS were reported by Benoit *et al.* [9] and by Dressler and Alan [10]. Using the transmission technique, Van Veen *et al.* [11] and Jordan and Burrow [12] also observed the π^* resonance in electron-acetaldehyde interaction.

Recently, grand-total cross sections (TCS) for electron scattering by acetaldehyde were measured in the 0.7–400 eV range by Szmytkowski [13]. His experimental results did not show evidence of shape resonances at energies below 6 eV. More recently, Gauf *et al.* [6] reported measured elastic differential cross sections (DCS) for e^--acetaldehyde collisions in the 1–50 eV range. At energies below 20 eV, their experimental fixed-angle DCS at some selected angles also did not reveal evidence of the π^* shape resonance.

Acetone is similar to acetaldehyde. As for acetaldehyde, the experimental investigation of electron-assisted processes involving acetone is also quite intense. Normalized total ionization cross sections (TICS) at 75 eV were reported by Otvos and Stevenson [14], Harrison *et al.* [15], and Beran and Kevan [16]. Absolute TICS were measured by Bull and Harland [17] in the 15–285 eV range. The negative ion formation by electron attachment to acetone was investigated by Dorman [18], Naff *et al.* [19], and Jordan and Burrow [12]. Experimental TCS for electron-acetone scattering in the 0.8–600 eV range were reported by Kimura *et al.* [20]. More recently, absolute TCS for electron-acetone collision were measured by Szmytkowski [13] in the 0.7–400 eV range. In addition, TCS for positron-acetone scattering in the 0.2–23 eV interval were recently reported by Zecca *et al.* [21]. Nevertheless, there is no reported measurement of the DCS for elastic electron scattering by acetone in the literature.

As for acetaldehyde, TCS reported by Szmytkowski [13] for acetone also did not present evidence of the π^* shape resonance at low incident energies. One possible reason is that both acetaldehyde and acetone are strongly polar targets; therefore the π^* shape resonance feature might be masked by the intense dipole-scattering background, as seen in our previous work on formamide [7]. In order to clarify this fact, the present paper reports a theoretical investigation on e^--acetone scattering. In our calculation, the dynamics of the projectile-target interaction is represented by a molecular complex optical potential (MCOP) at the static-exchange-polarization plus absorption (SEPA) level of approximation. This model has already been applied by our group to study electron collisions with other carbonyl-containing molecules, e.g., formaldehyde [3] and formamide [7]. Also, due to the lack of experimental DCS for this target, we performed measurements of this physical quantity in the 30–800 eV range using the relative-flow technique (RFT). The experimental elastic integral (ICS) and momentum-transfer cross sections (MTCS) are generated from the measured DCS via a numerical integration procedure.

The organization of this work is as follows: In Sec. II, we present briefly the experimental procedure. In Sec. III, the theory we used and details of the calculations are presented. In Sec. IV, we compare our calculated and measured data. Comparison with the experimental TCS of Kimura *et al.* [20] and Szmytkowski [13] and TICS of Bull and Harland [17] are also presented. Finally, some concluding remarks are also presented in that section.

II. EXPERIMENT

Measurements of the scattered-electron intensities were performed using a crossed electron-beam–molecular-beam geometry with the same procedure and experimental setup presented in our previous works [22–28]. The electron source used in our setup provides a beam in the 30–1000 eV range. This beam is perpendicular to the gas beam which is generated by a molybdenum tube with inner diameter $d = 1$ mm and aspect ratio $\gamma = d/L = 0.03$. Details of our gas manifold were described previously [25].

Acetone was purchased from Merk with purity better than 99%. For the measurements, approximately 1 mL of sample was transferred into a small glass vial attached to the gas manifold and underwent a treatment in order to eliminate atmospheric air through freeze-thaw cycles. The working pressure in the scattering chamber was kept typically at 5×10^{-7} Torr, and the pressure in the gas reservoir of the gas manifold was lower than 0.5 Torr. The purity of the sample was checked with a quadrupole residual gas analyzer attached to the scattering chamber. In addition, the vial containing the sample was kept in a bath with water and ice in order to ensure the gas-beam stability during the measurements.

The electronic inelastically scattered electrons were discriminated from those scattered elastically by using a retarding-field energy analyzer with resolution around 1.5 eV. This resolution does not allow the separation of the vibrationally elastic and inelastic processes; thus the measured intensities are vibrationally summed. The scattered intensities were converted to absolute DCS using the RFT [29]. For that, precise determination of the relative flows of both acetone and the secondary standards (argon and nitrogen) is required. Such flows were measured following the procedure already described [25]. Moreover, the DCS for N_2 at 30 eV reported by Shyn and Carignan [30], with quoted errors of 14%, and the DCS for Ar of Jansen *et al.* [31] in the 100–500 eV range, with quoted experimental uncertainties of 6.5%, were used to normalize our data. The absolute DCS for N_2 at 50 eV with experimental uncertainties of 19% and those for Ar at 800 eV with uncertainties of 12%, both from DuBois and Rudd [32], were used. The uncertainties quoted for the secondary standards plus those associated with the statistical nature of the measured scattering intensities of each gas (estimated to be 3%), the uncertainties of pressure fluctuations, electron-beam current readings, background scattering (estimated to be less than 2% each), and the uncertainty associated with the normalization procedure (6%) provided overall estimated uncertainties of 16.5% at 30 eV, 21% at 50 eV, 15% at 800 eV, and 11% elsewhere. The ICS and MTCS were obtained via a numerical integration over the DCS. An extrapolation procedure was used to estimate the DCS at scattering angles not covered experimentally. The trend of the theoretical results was followed in this procedure in order to reduce the arbitrariness. The overall uncertainties on ICS and MTCS were estimated to be 30% at 30 and 50 eV and 25% elsewhere.

III. THEORY AND NUMERICAL PROCEDURE

Since the theory used in this work has already been given in detail in several previous works [3,33,34], it will be presented only briefly. Basically, a complex optical potential $U_{\rm opt}$ composed of static (U_{st}), exchange (U_{ex}), correlation-polarization (U_{cp}), and absorption (U_{ab}) contributions is used to represent the electron-target interaction. This potential is divided in two parts, namely, U_1 and U_2. Then, the transition T matrix can also be written as

$$T = T_1 + T_2, \tag{1}$$

where

$$T_1 = \langle \phi(\vec{k}_f)|U_1|\psi_1^+(\vec{k}_i)\rangle \tag{2}$$

and

$$T_2 = \langle \psi_1^-(\vec{k}_f)|U_2|\psi^+(\vec{k}_i)\rangle. \tag{3}$$

In Eqs. (2) and (3), ϕ is the unperturbed plane wave, ψ is the solution of the Schrödinger scattering equation for the full optical potential $U_{\rm opt}$, ψ_1 is the solution of the distorted-wave Schrödinger equation for potential U_1, and k is the magnitude of the electron linear momentum. The partition of $U_{\rm opt}$ into U_1 and U_2 is arbitrary. In this work, we chose

$$U_1 = U_{st} + U_{ex}^{\rm loc} + U_{cp} \tag{4}$$

and

$$U_2 = U_{ex} - U_{ex}^{\rm loc} + iU_{ab}, \tag{5}$$

where $U_{ex}^{\rm loc}$ is a reduced local exchange potential.

By solving numerically the distorted-wave Schrödinger scattering equation with potential U_1, ψ_1 and T_1 are obtained. Further, T_2 is obtained iteratively using the $[N/N]$ Padé approximant technique [35]:

$$T_2[N/N] = -\sum_{i,j=1,N-1} \langle \psi_1^-|U_2|\phi^{(i)+}\rangle (D^{-1})_{ij} \langle \phi^{(j)-}|U_2|\psi_1^+\rangle, \tag{6}$$

where

$$D_{ij} = \langle \phi^{(i)-}|U_2 - U_2 G_1^+ U_2|\phi^{(j)+}\rangle \tag{7}$$

and G_1 is the distorted-wave Green's function, which satisfies the following condition:

$$(\nabla^2 + k^2 - U_1)G_1^{\pm}(\vec{r},\vec{r}') = \delta(\vec{r},\vec{r}'). \tag{8}$$

The superscripts $-$ and $+$ appearing in the above equations denote the incoming and outgoing boundary conditions of the scattering waves, respectively. In our calculation, the truncation parameter N was iteratively increased until convergence was achieved. The converged body-frame (BF) T matrix (or, equivalently, the BF scattering amplitude f) can then be expressed in the laboratory frame (LF) by the usual frame transformation [36].

TABLE I. Experimental DCS (in 10^{-16}cm^2/sr) and ICS and MTCS (in 10^{-16}cm^2) for elastic e^--acetone scattering.

Angle (deg)	E (eV)								
	30	50	100	150	200	300	400	500	800
10	31.40	52.28	33.64	24.33	16.91	11.78	7.63	7.27	4.60
15	17.84		7.10	7.39	3.94	4.04	3.14	3.17	2.01
20	8.46	8.45	2.76	3.24	2.24	1.99	1.59	1.47	1.24
25	4.58		1.44	1.92	1.33	0.923	0.963	1.04	0.548
30	2.66	1.67	1.09	1.02	0.746	0.765	0.789	0.656	0.249
35	2.16		0.767	0.723	0.668	0.601	0.501	0.359	0.178
40	1.73	1.06	0.591	0.499	0.494	0.396	0.268	0.256	0.120
50	1.43	0.680	0.365	0.364	0.259	0.179	0.157	0.120	0.052
60	1.04	0.398	0.268	0.194	0.156	0.136	0.098	0.078	0.030
70	0.855	0.261	0.172	0.126	0.129	0.092	0.066	0.051	0.020
80	0.672	0.199	0.129	0.137	0.098	0.071	0.055	0.034	0.015
90	0.582	0.175	0.110	0.120	0.077	0.050	0.039	0.028	0.011
100	0.523	0.184	0.142	0.115	0.059	0.049	0.035	0.022	0.010
110	0.599	0.209	0.160	0.129	0.046	0.044	0.030	0.018	0.009
120	0.621	0.264	0.187	0.136	0.036	0.039	0.025	0.016	0.007
ICS	22.4	20.1	12.4	9.7	8.6	5.7	4.4	4.1	2.9
MTCS	11.0	5.2	3.1	2.1	1.4	0.86	0.62	0.47	0.21

The ground-state Hartree-Fock self-consistent-field (HF-SCF) wave function of acetone was obtained using the triple-zeta valence (TZV-3d) basis set of the GAMESS package [37]. At the experimental molecular geometry [38], this basis provided a total energy of −192.022905 hartrees. The calculated electric dipole moment is 3.2080 D, in fairly good agreement with the

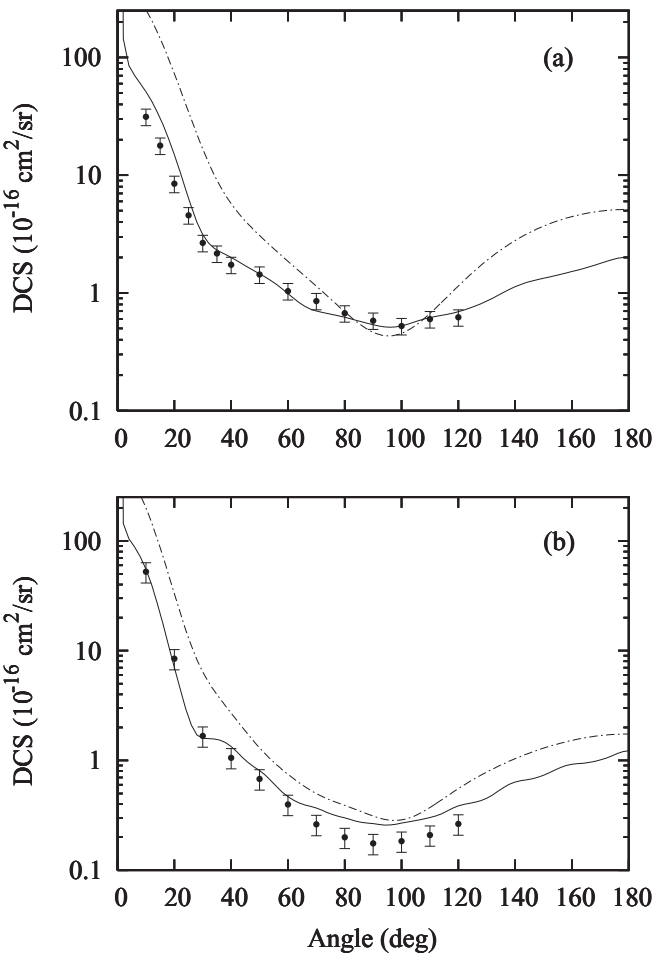

FIG. 1. DCS for elastic e^--acetone scattering at (a) 30 eV and (b) 50 eV. Solid curve, the present MCOP results; dash-dotted curve, the present IAM results; solid circles, the present experimental results.

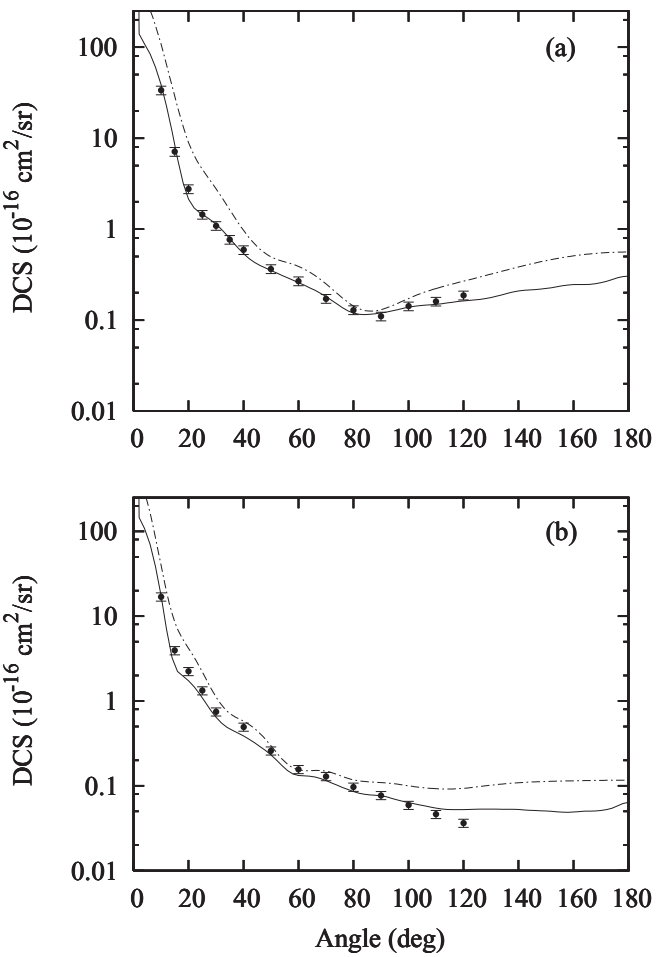

FIG. 2. Same as in Fig. 1, but at (a) 100 eV and (b) 200 eV.

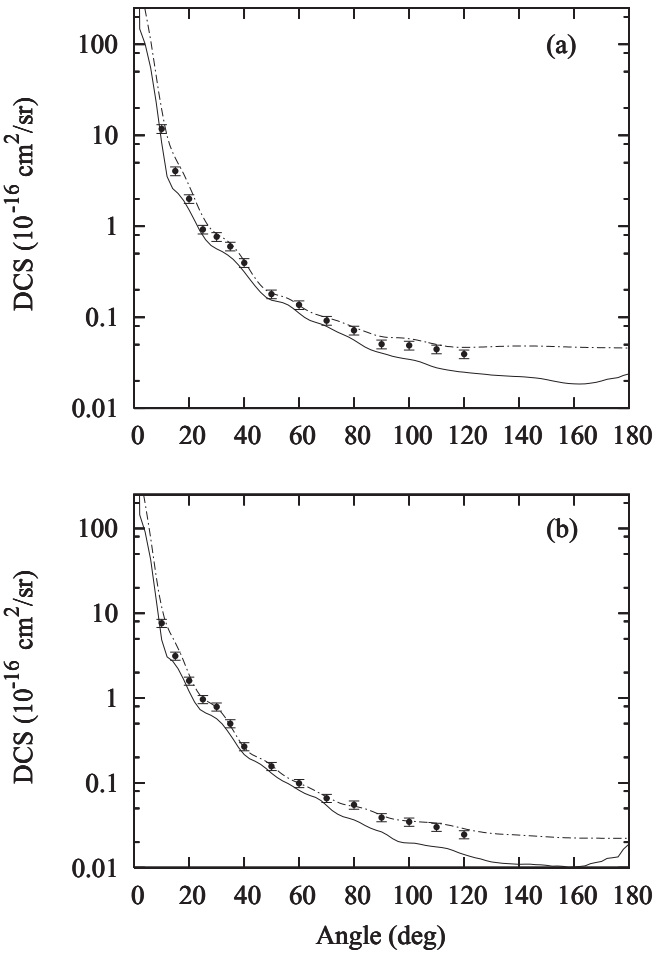

FIG. 3. Same as in Fig. 1, but at (a) 300 eV and (b) 400 eV.

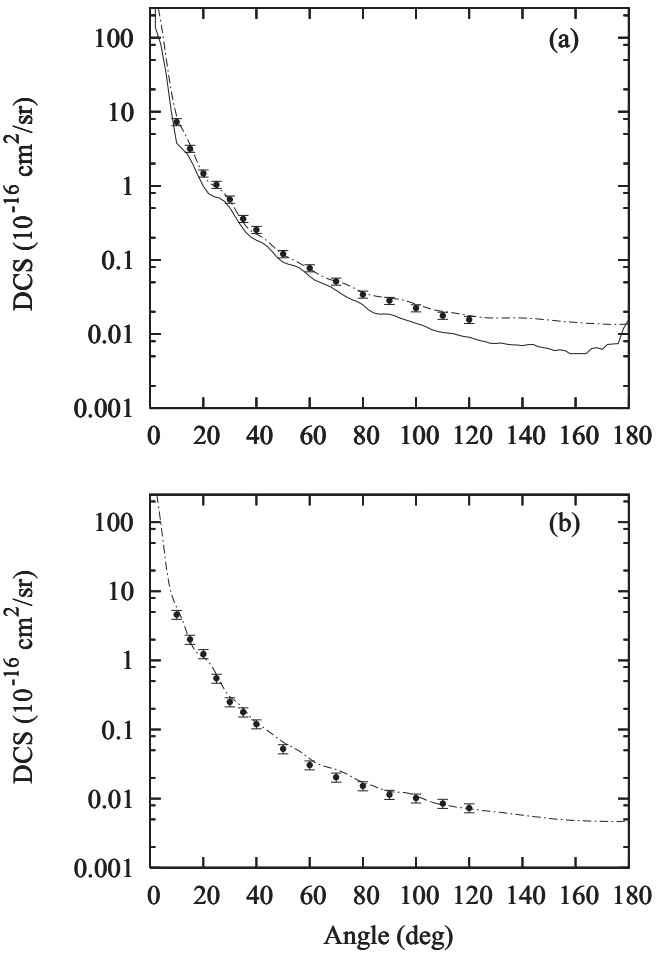

FIG. 4. Same as in Fig. 1, but at (a) 500 eV and (b) 800 eV.

experimental value of 2.88 D [38]. It is necessary to go beyond the HF level to obtain values closer to experimental data. The dipole polarizabilities calculated at the HF-SCF level using the same basis set are $\alpha_{xx} = 31.98$ a.u., $\alpha_{yy} = 41.10$ a.u., and $\alpha_{zz} = 42.60$ a.u., resulting in an average dipole polarizability of $\alpha_0 = 38.56$ a.u., in good agreement with the experimental value of 41.14 a.u. [38].

In the present work, U_{st} and U_{ex} were derived exactly from the target wave function, whereas U_{cp} was obtained in the framework of the free-electron-gas model, derived from a parameter-free local density, as prescribed by Padial and Norcross [39]. Our calculated polarizabilities are used to generate the asymptotic form of U_{cp}.

The absorption potential U_{ab} is the scaled quasifree scattering model (SQFSM) absorption potential of Lee *et al.* [40], which is an improvement of version 3 of the model absorption potential originally proposed by Staszewska *et al.* [41]. The Hara free-electron-gas-exchange potential [42] was used to generate the local exchange potential U_{ex}^{loc}.

In our calculation, the wave functions and interaction potentials, as well as the related matrices, are single-center expanded about the center of mass of the molecule in terms of the symmetry-adapted functions $X_{lh}^{p\mu}$ [43]. The truncation parameters used in these expansions were $l_c = 30$ and $h_c = 30$ for all bound and continuum orbitals, whereas the T-matrix elements were truncated at $l_c = 25$ and $h_c = 25$ for energies up to 50 eV and at $l_c = 30$ and $h_c = 30$ for higher energies. The calculated cross sections were converged at N up to 10.

Also, a Born-closure formula is used to account for the contribution of higher partial-wave components of the scattering amplitudes. This procedure is necessary due to the strongly polar nature of the target, as used in some of our previous studies [27,44,45].

IV. RESULTS AND DISCUSSION

Our experimental DCS, ICS, and MTCS for elastic electron scattering by acetone in the 30–800 eV range are listed in Table I. In Figs. 1–4, we present the comparison of the present experimental DCS with our calculated results in the 30–800 eV range. The present results calculated using the independent-atom model (IAM) [24] are also shown. In general there is good agreement between the present measured results and calculated MCOP data using the Padé approximant method, particularly at energies up to 300 eV. At higher energies, the theoretical MCOP results underestimate the DCS at large scattering angles. This discrepancy is mainly due to the lack of convergence in the single-center expansion of the nuclear part of the interacting potential for atoms a few angstroms away from the origin. Particularly at high incident energies,

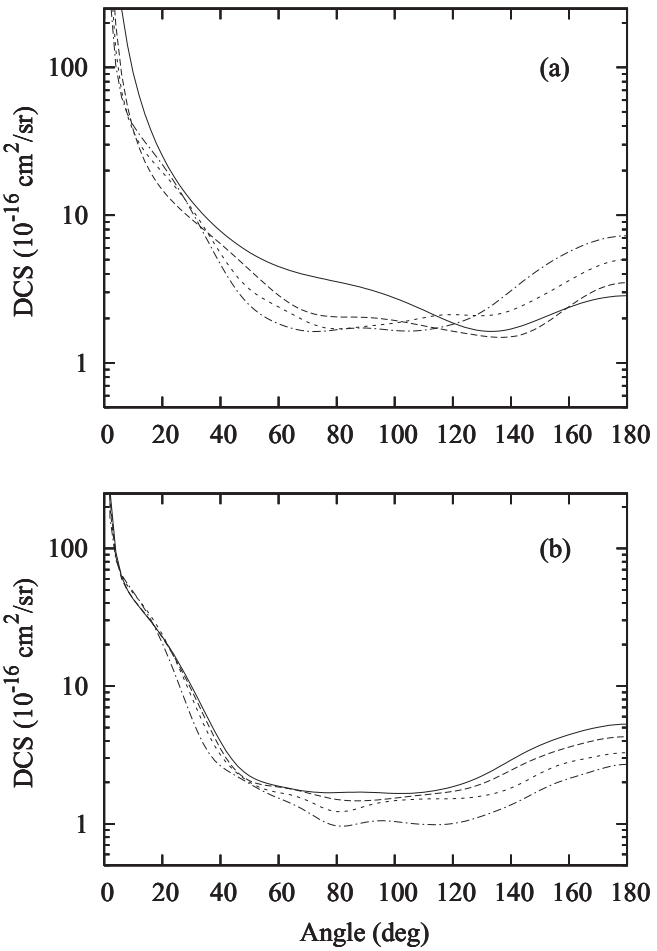

FIG. 5. Present MCOP DCS for elastic e^--acetone scattering. (a) Solid curve, at 1 eV; long-dashed curve, at 3 eV; short-dashed curve, at 5 eV; dash-dotted curve, at 8 eV. (b) Solid curve, at 10 eV; dashed curve, at 12 eV; short-dashed curve, at 15 eV; dash-dotted curve, at 20 eV.

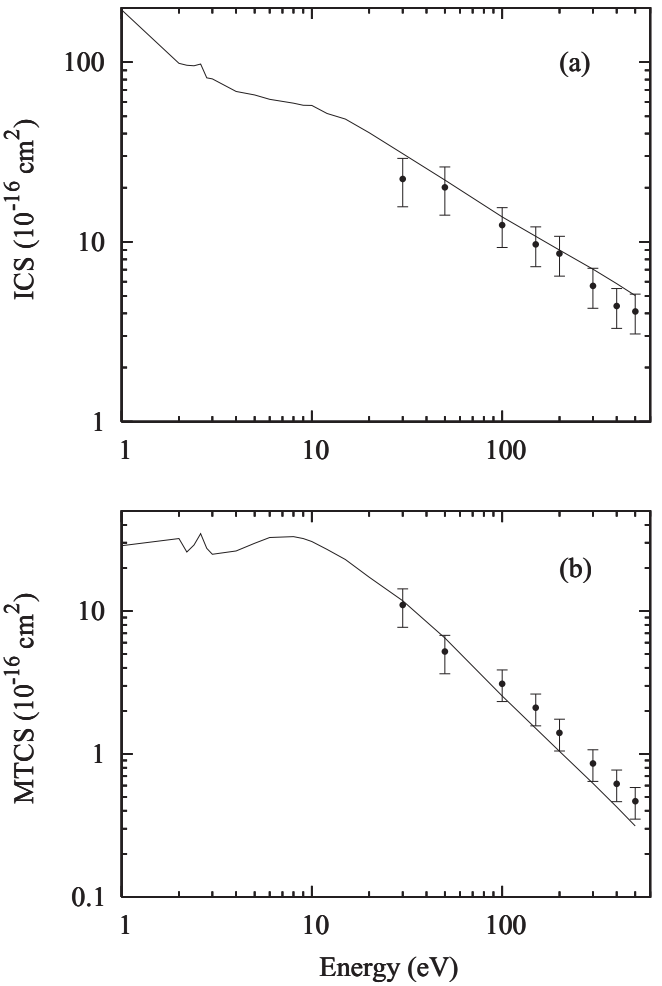

FIG. 6. (a) ICS and (b) MTCS for elastic e^--acetone scattering in the 1–500 eV range. Solid curve, present calculated data using the MCOP; solid circles, present experimental data.

the scattering electron penetrates deeply into the molecule and then would be more affected by that part of the potential. For a target like acetone, such convergence would be achieved only with very large values of l_c. The calculated results using the IAM lie systematically above the theoretical MCOP data. Nevertheless, the discrepancies diminish with increasing incident energies. At 100 eV and below, the IAM calculations also strongly overestimate the experimental DCS. However, it is interesting to note that for energies higher than 300 eV, the theoretical results calculated using the IAM are in better agreement with the measured data at large scattering angles due to the multicentric nature of the interaction potential used in these calculations [46]. Moreover, shallow oscillations seen in the experimental and in the theoretical DCS are due to the electron diffraction effects.

For the sake of completeness, in Fig. 5, we present some MCOP DCS in the 1–20 eV range. Unfortunately, there are no other results to compare with our data in this energy range. It is noted that the calculated DCS between 8 and 10 eV show some evidence of weak double-dip structure, indicating the possible occurrence of d-wave resonances.

In Fig. 6, we present our theoretical ICS and MTCS calculated using the MCOP for electron scattering by acetone in the 1–500 eV range. The present experimental results of ICS and MTCS in the 30–500 eV range are also shown for comparison. In general, there is reasonable agreement between our calculated and measured data in the entire energy range where comparison is made. At low incident energies, our calculated ICS and MTCS show a small peak at incident energy around 2.6 eV and a broad resonance-like feature centered at about 8 eV. These features are more visible in the calculated MTCS than in ICS. In order to clarify the physical nature of these features, we present in Figs. 7(a) and 7(b) the partial ICS (without Born correction) and the eigenphase sums. From these figures, it is clearly seen that the peak located at 2.6 eV is due to a strong $^2B_2$ ($^2\pi^*$) resonance, whereas the broad feature located at about 8 eV is a combination of weak $^2B_1$ and $^2A_2$ resonances (both at around 8 eV) and a weak $^2A_1$ shape resonance at around 10 eV. Probably, the double-dip behavior seen in our calculated DCS in the 8–10 eV range can be associated with these resonances. Unfortunately, our measurement does not cover incident energies below 30 eV,

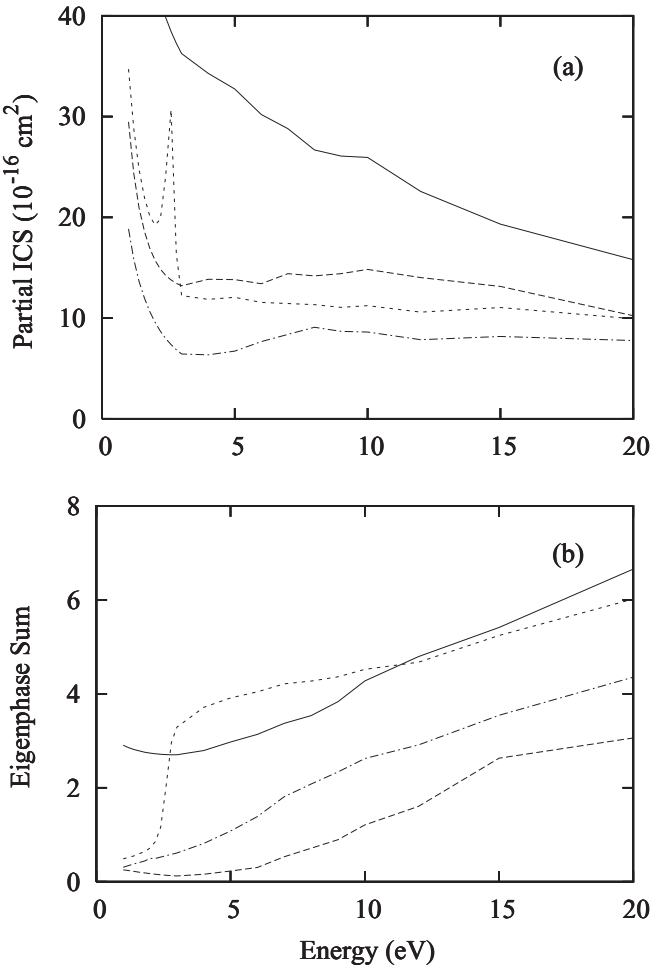

FIG. 7. Present partial-channel (a) ICS and (b) eigenphase sums calculated using the MCOP for elastic e^--acetone scattering in the 1–20 eV energy range. Solid curve, A_1 symmetry; dash-dotted curve, A_2 symmetry; long-dashed curve, B_1 symmetry; short-dashed curve, B_2 symmetry.

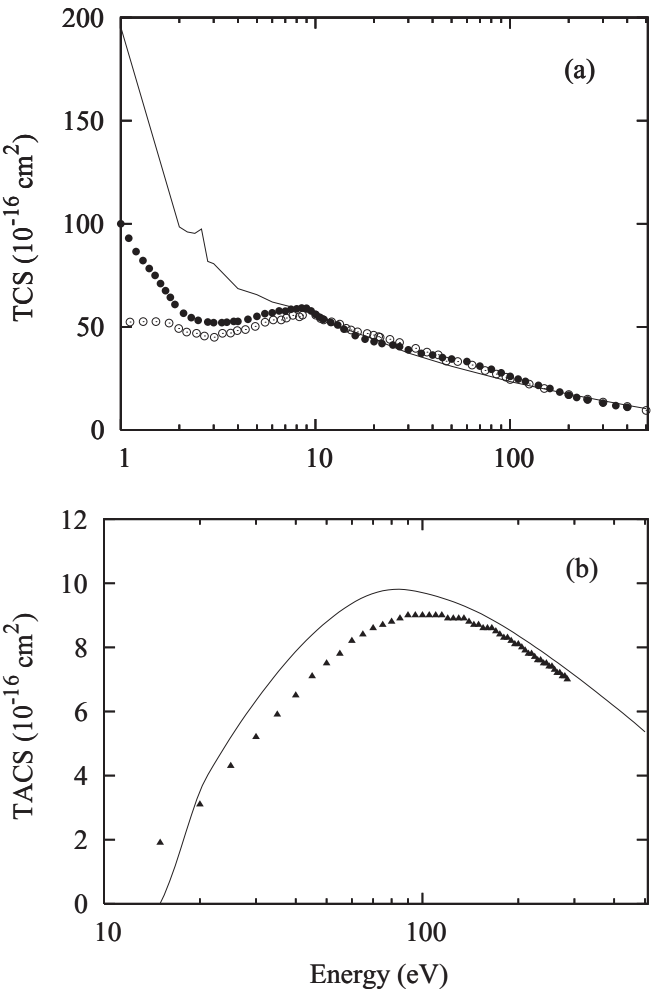

FIG. 8. (a) TCS and (b) TACS for e^--acetone scattering in the 1–500 eV range. Solid curve, present data calculated using the MCOP; solid circles, experimental data of Szmytkowski [13]; open circles, experimental data of Kimura *et al.* [20]; triangles, experimental data for TICS of Bull and Harland [17].

and also there are no other experimental data in the literature to compare with our calculations.

In Fig. 8(a), we present our theoretical TCS for electron scattering by acetone in the 1–500 eV range. The experimental TCS of Kimura *et al.* [20] in the 1–500 eV range and of Szmytkowski [13] in the 1–400 eV range are also shown for comparison to our data. Both experimental results show a bump at around 8 eV, which agrees with our theoretical prediction. This resonance was also seen in electron scattering by hydrocarbon experiments and is of a $k\sigma^*$ nature, as already discussed by Kimura *et al.* [20]. Quantitatively, there is also good agreement between our calculated results and the measured data at 10 eV and above. Nevertheless, the $^2B_2$ resonance located at about 2.6 eV predicted by our calculation is not seen in the TCS measured by Szmytkowski [13]. The TCS of Kimura *et al.* has shown a small shoulder at about 1.5 eV which may be due to the $^2B_2$ ($^2\pi^*$) resonance but shifted to lower incident energies. Moreover, our calculation overestimates both experimental TCS, particularly at energies below 3 eV. There is also a strong disagreement between the two sets of experimental data in this energy region. Such discrepancies are somewhat expected due to the difficulties associated with the measurements of TCS for strongly polar targets at low incident energies.

In Fig. 8(b), the present total absorption cross sections (TACS) are compared with the experimental TICS of Bull and Harland [17] in the 15–285 eV energy range. In general, there is very good qualitative agreement between the calculated TACS and experimental TICS. Quantitatively, our TACS lie above the TICS in the entire energy range, except at 15 eV. Since TACS account for both excitation and ionization processes, whereas only ionization processes are accounted for in TICS, the above behavior is then expected.

In summary, in this study, we reported a joint theoretical-experimental investigation of electron collisions with acetone in a wide energy range. More precisely, absolute DCS, ICS, and MTCS for elastic e^--acetone scattering were investigated experimentally in the 30–800 eV range. The present study was mainly motivated by the lack of experimental cross-section data for this target in the literature. Our measured data are in generally good agreement with our theoretical

data calculated using the MCOP model. Moreover, although a sharp resonance in the $^2B_2$ scattering channel at about 2.6 eV was revealed in our calculations, as seen in Fig. 7(a), it becomes a small peak in the calculated ICS and MTCS curves. The main reason for this fact is the strong contribution of the structureless dipole interaction in the calculated ICS and MTCS at low incident energies, which has masked the resonance peak. Also, the absence of clear evidence of the occurrence of this resonance in the experimental TCS of Kimura *et al.* [20] and Szmytkowski [13] may also be caused by the vibrational motion of the target. In fact, we have performed a simulation of the vibrational effects of the carbonyl group on this resonance. In this simulation, we have fixed the equilibrium geometry of the target except for the C=O bond, which is allowed to vary. The $^2B_2$ resonances are calculated at five C=O internuclear distances ($r = r_{eq} + \Delta r$, with $\Delta r = -0.12, -0.06, 0.0, 0.06$, and 0.12 Å). It was seen that both the height and the width of the resonance changed with the bond length. Nevertheless, the vibrational-averaged ICS calculated using harmonic-oscillator vibrational wave functions showed only a very small broadening of the resonant peak.

ACKNOWLEDGMENTS

The authors would like to thank Dr. A. S. dos Santos, L. M. F. de Oliveira, and G. E. O. Camargo for their valuable help. This research was partially supported by the agencies CNPq (Brazil), FAPESP (Brazil), and CAPES (Brazil).

[1] T. N. Rescigno, C. W. McCurdy, and B. I. Schneider, Phys. Rev. Lett. **63**, 248 (1989).
[2] S. Kaur and K. L. Baluja, J. Phys. B **38**, 3917 (2005).
[3] J. R. Ferraz, A. S. dos Santos, G. L. C. de Souza, A. I. Zanelato, T. R. M. Alves, M.-T. Lee, L. M. Brescansin, R. R. Lucchese, and L. E. Machado, Phys. Rev. A **87**, 032717 (2013).
[4] M. H. F. Bettega, Phys. Rev. A **74**, 054701 (2006).
[5] C. S. Trevisan, A. E. Orel, and T. N. Rescigno, Phys. Rev. A **74**, 042716 (2006).
[6] A. Gauf, C. Navarro, G. Balch, L. R. Hargreaves, M. A. Khakoo, C. Winstead, and V. McKoy, Phys. Rev. A **89**, 022708 (2014).
[7] M. G. P. Homem, I. Iga, G. L. C. de Souza, A. I. Zanelato, L. E. Machado, J. R. Ferraz, A. S. dos Santos, L. M. Brescansin, R. R. Lucchese, and M.-T. Lee, Phys. Rev. A **90**, 062704 (2014).
[8] C. Benoit and R. Abouaf, Chem. Phys. Lett. **123**, 134 (1986).
[9] C. Benoit, R. Abouaf, and S. Cvejanovic, Chem. Phys. **117**, 295 (1987).
[10] R. Dressler and M. Allan, J. Electron Spectrosc. Relat. Phenom. **41**, 275 (1986).
[11] E. H. van Veen, W. L. van Dijik, and H. H. Brongersma, Chem. Phys. **16**, 337 (1976).
[12] K. D. Jordan and P. D. Burrow, Acc. Chem. Res. **11**, 341 (1978).
[13] C. Szmytkowski, J. Phys. B **43**, 055201 (2010).
[14] J. W. Otvos and D. P. Stevenson, J. Am. Chem. Soc. **78**, 546 (1956).
[15] A. G. Harrison, E. G. Jones, S. K. Gupta, and G. P Nagy, Can. J. Chem. **44**, 1967 (1966).
[16] J. A. Beran and L. Kevan, J. Phys. Chem. **73**, 3866 (1969).
[17] J. N. Bull and P. W. Harland, Int. J. Mass Spectrom. **273**, 53 (2008).
[18] F. H. Dorman, J. Chem. Phys. **44**, 3856 (1966).
[19] W. T. Naff, R. N. Compton, and C. D. Cooper, J. Chem. Phys. **57**, 1303 (1972).
[20] M. Kimura, O. Sueoka, A. Hamada, and Y. Itikawa, Adv. Chem. Phys. **111**, 537 (2007).
[21] A. Zecca, L. Chiari, E. Trainotti, A. Sarkar, and M. J. Brunger, PMC Phys. B **3**, 4 (2010).
[22] I. Iga, M. T. Lee, M. G. P. Homem, L. E. Machado, and L. M. Brescansin, Phys. Rev. A **61**, 022708 (2000).
[23] P. Rawat, I. Iga, M. T. Lee, L. M. Brescansin, M. G. P. Homem, and L. E. Machado, Phys. Rev. A **68**, 052711 (2003).
[24] M. G. P. Homem, R. T. Sugohara, I. P. Sanches, M. T. Lee, and I. Iga, Phys. Rev. A **80**, 032705 (2009).
[25] M. G. P. Homem, I. Iga, R. T. Sugohara, I. P. Sanches, and M. T. Lee, Rev. Sci. Instrum. **82**, 013109 (2011).
[26] R. T. Sugohara, M. G. P. Homem, I. P. Sanches, A. F. de Moura, M. T. Lee, and I. Iga, Phys. Rev. A **83**, 032708 (2011).
[27] M.-T. Lee, G. L. C. de Souza, L. E. Machado, L. M. Brescansin, A. S. dos Santos, R. R. Lucchese, R. T. Sugohara, M. G. P. Homem, I. P. Sanches, and I. Iga, J. Chem. Phys. **136**, 114311 (2012).
[28] R. T. Sugohara, M. G. P. Homem, I. Iga, G. L. C. de Souza, L. E. Machado, J. R. Ferraz, A. S. dos Santos, L. M. Brescansin, R. R. Lucchese, and M.-T. Lee, Phys. Rev. A **88**, 022709 (2013).
[29] S. K. Srivastava, A. Chutjian, and S. Trajmar, J. Chem. Phys. **63**, 2659 (1975).
[30] T. W. Shyn and G. R. Carignan, Phys. Rev. A **22**, 923 (1980).
[31] R. H. J. Jansen, F. J. de Heer, H. J. Luyken, B. van Wingerden, and H. J. Blaauw, J. Phys. B **9**, 185 (1976).
[32] R. D. DuBois and M. E. Rudd, J. Phys. B **9**, 2657 (1976).
[33] P. Rawat, M. G. P. Homem, R. T. Sugohara, I. P. Sanches, I. Iga, G. L. C. de Souza, A. S. dos Santos, R. R. Lucchese, L. E. Machado, L. M. Brescansin, and M.-T. Lee, J. Phys. B **43**, 225202 (2010).
[34] G. L. C. de Souza, M.-T. Lee, I. P. Sanches, P. Rawat, I. Iga, A. S. dos Santos, L. E. Machado, R. T. Sugohara, L. M. Brescansin, M. G. P. Homem, and R. R. Lucchese, Phys. Rev. A **82**, 012709 (2010).
[35] F. A. Gianturco, R. R. Lucchese, and N. Sanna, J. Chem. Phys. **102**, 5743 (1995).
[36] A. R. Edmonds, *Angular Momentum and Quantum Mechanics* (Princeton University Press, Princeton, NJ, 1960).
[37] M. W. Schmidt, K. K. Baldridge, J. A. Boatz, S. T. Elbert, M. S. Gordon, J. H. Jensen, S. Koseki, N. Matsunaga, K. A. Nguyen, S. Su, T. L. Windus, M. Dupuis, and J. A. Montgomery, J. Comput. Chem. **14**, 1347 (1993).
[38] Computational Chemistry Comparison and Benchmark DataBase, http://cccbdb.nist.gov.

[39] N. T. Padial and D. W. Norcross, Phys. Rev. A **29**, 1742 (1984).
[40] M.-T. Lee, I. Iga, L. E. Machado, L. M. Brescansin, E. A. y Castro, I. P. Sanches, and G. L. C. de Souza, J. Electron Spectrosc. Relat. Phenom. **155**, 14 (2007).
[41] G. Staszewska, D. W. Schwenke, and D. G. Truhlar, Phys. Rev. A **29**, 3078 (1984).
[42] S. Hara, J. Phys. Soc. Jpn. **22**, 710 (1967).
[43] P. G. Burke, N. Chandra, and F. A. Gianturco, J. Phys. B **5**, 2212 (1972).
[44] L. M. Brescansin, L. E. Machado, M.-T. Lee, H. Cho, and Y. S. Park, J. Phys. B **41**, 185201 (2008).
[45] L. E. Machado, L. M. Brescansin, I. Iga, and M.-T. Lee, Eur. Phys. J. D **33**, 193 (2005).
[46] M.-T. Lee and L. C. G. Freitas, J. Phys. B **13**, 233 (1983).